

Rotational stability of plasma blobs

D. A. D'Ippolito, J. R. Myra, and D. A. Russell

Lodestar Research Corporation, 2400 Central Avenue, Boulder, Colorado 80301

G. Q. Yu

University of California, San Diego, California

March, 2004; revised May, 2004
(submitted to Physics of Plasmas)

DOE/ER/54392-25

LRC-04-97

LODESTAR RESEARCH CORPORATION

Rotational stability of plasma blobs

D. A. D'Ippolito,[†] J. R. Myra, and D. A. Russell

Lodestar Research Corporation, 2400 Central Avenue, Boulder, Colorado 80301

G. Q. Yu

University of California, San Diego, California

Abstract

The stability of plasma blobs which have both density and temperature higher than the surrounding plasma, and can transport heat as well as particles, is considered. It is shown that the internal blob temperature profile $T_e(r)$ can drive azimuthal rotation or spin $v_\theta(r)$ about the blob axis, which produces a robust $m = 2$ rotational instability in the interchange limit ($k_\parallel = 0$). The theory includes the effects of the centrifugal and Coriolis forces, the sheared velocity $v_\theta(r)$, and the axial sheath boundary condition. Estimates show that finite-Larmor-radius stabilization is ineffective, but the sheath conductivity can be strongly stabilizing. The blob rotational instability has only a small direct impact on the particle and energy transport, but it serves as a useful diagnostic for the underlying blob spin, which is an important variable in determining the blob's radial velocity. A separate branch of temperature-gradient-driven sheath instabilities, predicted in the eikonal limit, is not observed for low mode numbers.

PACS numbers: 52.25.Fi, 52.35.Ra, 52.55.Dy, 52.55.Fa

[†]email: dasd@lodestar.com

I. Introduction

The study of coherent objects arising in turbulence has a long history. In the plasma physics context, Horton showed that large amplitude turbulence tends to form coherent vortices¹ when the amplitude of the potential and vorticity (related to the spin around the central axis) is sufficiently large compared to the linear growth rate of the underlying turbulence. Under certain conditions, dipolar vortices (corresponding to charge dipoles) were found in his two-dimensional (2D) simulations. More recently another model of coherent turbulent objects called “blobs”, which also involve charge dipoles, has been studied.^{2,3} A blob is defined as a plasma filament with a higher density and possibly higher temperature than the surrounding scrape-off-layer (SOL) plasma; it varies slowly along the magnetic field but rapidly across it so that the filament looks like a “blob” in the plane perpendicular to \mathbf{B} . The extensive experimental motivation⁴⁻¹² for this model, the details of the 2D theory, and the implications for fusion devices of blob transport have been described in these references and in a recent short review paper.¹³

The blob model extends the earlier work on turbulent coherent objects by considering the sources and sinks for the dipolar charge. It was shown^{2,3} that an outwards force \mathbf{F} (e.g. due to toroidal curvature in a tokamak) produces a charge separation and resulting charge dipole in the $\mathbf{F}\times\mathbf{B}$ direction through the charge-dependent $\mathbf{F}\times\mathbf{B}$ drift. Experimentally and in computer simulations, the monopole density concentration in the blob is always accompanied by a charge dipole. The electric field \mathbf{E} created by this charge dipole leads to radial transport of the blob as a coherent object, which passively convects both particles and energy towards the wall, via the $\mathbf{E}\times\mathbf{B}$ drift. The magnitude of \mathbf{E} is determined by the balancing of the particle drift source with two sinks: the loss of charge by current flow J_{\parallel} along the field lines to the divertor sheaths,^{2,3} and the mixing of the positive and negative charges by blob spin around its axis, which act to reduce the internal charge polarization.¹⁴ Thus, the internal blob spin is an important dynamical variable. The formation and stability of blobs to curvature-driven secondary

instabilities^{15,16} is enhanced by the blob spin but its radial transport is hindered by the spin by partially defeating the internal charge polarization.¹⁴

Blobs develop spin when two conditions are satisfied: (i) the parallel transport of charge and energy to the sheaths is sufficiently rapid to suppress parallel variation of the electrostatic potential and temperature along B ($k_{\parallel} = 0$), and (ii) the blob has an internal temperature profile $T_e(r)$, where r is the blob radial coordinate. The case of interest here is a cylindrically-symmetric blob with a hot dense core, so that both $n(r)$ and $T_e(r)$ are monotonically decaying profiles. The first condition ensures that the blob is electrically connected to the sheath and thus has a large Bohm sheath potential, $e\Phi_B(r) = C_B T_e(r)$, where $C_B = \ln[(m_i/2\pi m_e)^{1/2}] \approx 3$ and the temperature is measured at the sheath. The second condition ensures that this potential produces a radial electric field in the blob and azimuthal spin around its axis. Early work on blob theory was concerned with the far SOL where the blobs are in thermal equilibrium with the background plasma due to the rapid parallel heat transport. In this limit, $T_e = \text{const.}$ and the blobs did not spin. More recent work has the goal of understanding blob properties near the separatrix, where the blobs have not yet had time to lose their hot interiors by parallel heat transport. This work is relevant to understanding the blob-like objects thrown off by ELMs,^{9,17,18} which have central densities and temperatures characteristic of the top of the pedestal, much denser and hotter than the surrounding SOL plasma.

In addition to the physics mentioned above, blob spin can also drive internal rotational instabilities that can tear the blob apart. This is the subject of the present paper. The theory of rotational instabilities of fusion plasmas has a long history.¹⁹⁻²² The goal of the present work is to apply this well-known theory to determine whether rotational instabilities of a hot blob, driven by its own internal spin, play a role in determining its dynamics and the associated SOL particle and energy transport. We also carry out a simple extension of the theory to include sheath effects that are important in the SOL. Another motivation for this study is to determine the qualitative and quantitative properties of the dominant rotational mode so that it can be used as a "signature" of blob spin (and thus of sheath connection) in interpreting visual 2D blob data, such as provided

by the gas puff imaging diagnostic.^{10,12} This study is restricted to the $k_{\parallel} = 0$ limit in which blob spin is expected to be large. The instability is driven by a combination of centrifugal force, Coriolis, Kelvin-Helmholtz and rotational shear effects. Both linear stability calculations and the result of a 2D simulation are presented.

When sheath conductivity is included in the analysis, the stability equation also includes the Berk-Ryutov-Tsidulko (BRT) ∇T_e -driven instabilities²³ in the eikonal limit. In the low mode number limit of interest here, the sheath conductivity term turns out to have a net stabilizing effect.

The plan of this paper is as follows. Section II discusses the characteristic time scales and growth rates. The stability equations are given in Sec. III, and the linear and nonlinear stability results are presented in Sec. IV. A summary and discussion of the main results of the paper is given in Sec. V.

II. Scaling of instability growth rates

We begin by comparing the scaling of the growth rate γ_R of the rotational instability with those of the dominant instabilities in the absence of spin: the sheath-interchange mode^{15,16} (γ_{SI}) and the Kelvin-Helmholtz (KH) mode¹⁶ driven by the sheared velocity $v_x(y)$ with growth rate γ_{KH} . (In this paper, x and y refer to the local radial and poloidal coordinates in the tokamak outer midplane.) The relative scaling of the growth rates determines the parameter regime in which the rotational mode dominates.

Here, we consider only the internal temperature profile $T_e(r)$ of the cylindrically-symmetric blobs and neglect the temperature variation $T_e(x)$ of the external background plasma, assuming that the latter varies on a scale length much longer than the blob radius a . For a hot blob, the radially decaying sheath potential implies a radial electric field with $E_r > 0$, which causes the blob to rotate in the azimuthal or θ direction with an angular frequency $\Omega(r) = v_{\theta}(r)/r$. The resulting centrifugal, Coriolis, and velocity-shear effects can drive low azimuthal-mode-number instabilities with eigenfunctions varying like $\psi(r) e^{im\theta}$. Here, (r, θ, z) are used to represent the cylindrical blob coordinates and no

variation in the axial coordinate z (parallel to \mathbf{B}) is assumed in either the equilibrium or stability analysis.

The blob stability can be described by the $B_\theta = 0$, $k_\parallel = 0$, $\beta_t = 8\pi p/B^2 = 0$ limits of the Freidberg-Pearlstein theory²² developed for theta-pinches. In Ref. 22, a radial differential equation (given in the next section) and an associated variational principle are given which include rotational, finite-Larmor radius (FLR), and line bending ($k_\parallel \neq 0$) effects. Balancing the driving term against the inertial term in the variational principle gives the following (dimensional) scaling of the growth rate:

$$\gamma^2 \approx \left(\frac{k_\theta}{k_\perp} \right)^2 \left(\frac{a}{L_n} \right) \Omega \Omega_E. \quad (1)$$

Here $k_\theta = m/r$, $\Omega = v_\theta/r$ is the angular rotation frequency, $\Omega_E = -cE_r/rB \approx (c/rB)(d\Phi_B/dr)$ is the $\mathbf{E} \times \mathbf{B}$ rotation frequency, and $\Phi_B \approx 3T_e$. In the presence of FLR effects [$\Omega_* \equiv -c/(ernB)(dp_i/dr) \neq 0$], the angular frequencies are related by the equilibrium radial force balance condition:

$$\Omega = \Omega_E - \Omega_*, \quad (2)$$

where $\tau = -\Omega_*/\Omega_E \sim T_i/T_e$ is the FLR parameter. Since $E_r > 0$ and $dp_i/dr < 0$ for the blob, both terms in Eq. (2) have the same sign and the diamagnetic drift Ω_* increases the instability drive, $\Omega = \Omega_E(1 + \tau)$ with $\tau > 0$. There is also an explicit FLR stabilization term ($\propto \Omega_*^2$) in the variational principle. A necessary condition for FLR stabilization is that the τ^2 term be larger than the (destabilizing) τ term, which requires $\tau \gg 1$. Thus, FLR stabilization of blobs is more difficult than in the well-known theta pinch problem for which $\tau \sim 1$ is sufficient to obtain stability. This conclusion is supported by our numerical calculations with the radial eigenmode equation including FLR effects derived in Ref. 22; FLR stabilization of the dominant rotational mode was found to be weak for $T_i/T_e < 10$. For this reason, in the remainder of this paper we will restrict the discussion to the case with $T_i/T_e = 0$.

Neglecting Ω_* and assuming that the sheath potential decays over a blob radius a , we can estimate the magnitude of the rotation and the growth rate. Setting $L_n \sim L_T \sim a$ and $k_\perp \sim k_\theta$, the rotational growth rate γ_R has the following dimensional scaling:

$$\gamma_R \sim \Omega \sim \left(\frac{\rho_s}{a} \right)^2 \Omega_i . \quad (3)$$

In dimensionless notation³ where velocity, frequency, and length, are normalized to the sound speed $c_s = (T_e/m_i)^{1/2}$, cyclotron frequency $\Omega_i = eB/m_i c$, and gyroradius $\rho_s = c_s / \Omega_i$, respectively, Eq. (3) becomes $\gamma_R \sim 1/a^2$. Using results from previous papers,^{15,16} the comparison with the sheath-interchange growth rate γ_{SI} and the Kelvin-Helmholtz (KH) growth rate γ_{KH} is

$$\gamma_R \sim \frac{C_B}{a} , \quad \gamma_{SI} \sim \frac{m^2 q}{a^3} , \quad \gamma_{KH} \sim \frac{q}{a} , \quad (4)$$

where C_B is the Bohm sheath coefficient defined earlier, $q = L_\parallel/R$ and a is the cylindrical blob radius in the plane perpendicular to \mathbf{B} . The KH mode referenced in Eq. (4) is a global (low- m) mode driven by the curvature-driven sheared flow, $v_x(y)$, for a blob propagating radially across a background plasma,¹⁶ and the growth rate is estimated as $\gamma \sim v_x/L_y \sim q/a^3$ using the 2D blob model result^{2,3} that $v_x = q/a^2$. There is also a KH instability associated with the rotation, which has a growth rate $\gamma \sim v_\theta/r \sim \Omega \sim C_B/a^2$, comparable to the mode driven by the centrifugal force. The numerical solutions of Sec. IV include the effects of the azimuthal rotational shear $v_\theta(r)$. For the remainder of this paper, we will not distinguish between the centrifugal and velocity-shear drives associated with rotation and will simply refer to both of these as rotational instabilities.

The main conclusion to draw from Eq. (4) is that the rotational growth rate is dominant for larger blobs and lower mode numbers m . Comparing the rotational and sheath-interchange growth rates for a fixed blob size, we find that $\gamma_R > \gamma_{SI}$ for

$$m < m_{\text{crit}} \sim (C_B a / q)^{1/2} , \quad (5)$$

which is also the condition to neglect the curvature term in the vorticity equation. High- m modes that violate Eq. (5) would be radially localized near the outside of the blob and would not affect the transport of the main body of the blob in a substantial way.

Finally, one can also show that the rotational growth rate is large compared to the blob convection rate γ_c ,¹⁵ defined as $\gamma_c = 1/\tau_c$, where $\tau_c = a/v_x \sim a^3$ is the time for the blob to convect one blob radius. Thus, $\gamma_R/\gamma_c \sim a$ is large for typical blobs (having $a \gg 1$ in units of the gyroradius) and the rotational instability is fast enough, in principle, to affect the blob transport.

III. Model Equations

The theory of propagating density blobs and their stability is based on a simple set of dimensionless equations that expresses the conservation of vorticity (charge), density, and temperature:^{2,3}

$$\nabla \cdot \left(n \frac{d}{dt} \nabla_{\perp} \Phi \right) = \alpha n T^{-1/2} (\Phi - \Phi_B) - \beta \nabla_y (nT), \quad (6)$$

$$\frac{dn}{dt} + \alpha T^{1/2} n = 0, \quad (7)$$

$$\frac{dT}{dt} + \alpha_T T^{3/2} = 0, \quad (8)$$

$$\frac{d}{dt} = \frac{\partial}{\partial t} + \mathbf{v} \cdot \nabla, \quad (9)$$

where Φ is the total electrostatic potential, Φ_B is the Bohm sheath potential, and the first term on the right-hand-side (rhs) of the vorticity equation was expanded in the limit $\varphi = \Phi - \Phi_B \ll 1$. Also, n is the particle density ($n = n_e = n_i$), $T = T_e$ is the electron temperature, $T_i = 0$ (neglect FLR and diamagnetic effects), $\alpha = (2\rho_s/L_{\parallel})$ measures the net parallel current and particle loss into the sheaths, α_T gives the energy loss into the sheaths, and $\beta = (2\rho_s/R)$ is the curvature parameter. In the blob model the velocity is given by the $\mathbf{E} \times \mathbf{B}$ drift, $\mathbf{v} = \mathbf{b} \times \nabla \Phi = \mathbf{e}_z \times \nabla \Phi$. To make the equations dimensionless, time

has been normalized to Ω_i^{-1} , length scales to ρ_s , and other quantities to reference values (e.g. separatrix values n_s and T_{es}).

Note that these equations apply in the *moderate-collisionality*, sheath-limited regime in which rapid electron conductivity along the field lines causes the electron temperature and electrostatic potential to be constant (flute approximation) and the sheath conductivity term [α term in Eq. (6)] to scale like $T_e^{-1/2}$.

We assume that the plasma filaments are localized perpendicular to \mathbf{B} and employ a slab model with orthogonal coordinates (x, y, z) to represent the tokamak geometry. Here, the curvature is written as $\boldsymbol{\kappa} = -(\rho_s/R) \hat{\mathbf{e}}_x$ with x in the direction of the major radius R . The z coordinate is taken along the direction of \mathbf{B} , so that $2\mathbf{b} \times \boldsymbol{\kappa} \cdot \nabla = -\beta \nabla_y$ and y is approximately in the poloidal direction at the outer midplane. Here, $y = 0$ denotes the location of the outer midplane and $x > 0$ corresponds to the SOL, so that motion in the positive x direction is outwards towards the wall. For the stability analysis, we also introduce the corresponding cylindrical blob coordinate system (r, θ, z) .

Several approximations are used to simplify the linear stability analysis. We consider time scales smaller than the parallel loss times, $t \ll \alpha_T^{-1} \ll \alpha^{-1}$, so that the rhs of Eqs. (7) and (8) can be neglected. This restricts the validity of the stability analysis to growth rates satisfying $\gamma \sim \Omega \gg \alpha_T$. With this approximation, we observe that the temperature equation (8) can be solved by the ansatz:

$$T = n^{\nu}. \quad (10).$$

We also neglect the curvature term ($\propto \beta$) in Eq. (6), as detailed studies of curvature-driven blob instabilities have already been published^{15,16} and we would like to focus here on the properties of instabilities driven only by rotation. The neglect of curvature is justified for large blobs satisfying Eq. (5). The combined effect of curvature and rotation is contained in the nonlinear 2D simulation discussed in Sec. IV.

The power law temperature profile in Eq. (10) is one example of the general class of "aligned" n and T profiles satisfying $T = T(n)$. The physical justification for this assumption is that the blob convects both the density and temperature of its birthplace

outwards across the SOL so that there is a correlation between the central blob density and temperature. From a theoretical point of view, this assumption has the advantage that the temperature equation is automatically satisfied by the solution to the continuity equation.

Using these approximations and combining Eqs. (6) and (7), we obtain the following set of reduced equations as a starting point for the rotational stability analysis:

$$\nabla \cdot \left(n \frac{d}{dt} \nabla_{\perp} \Phi \right) = \alpha n T^{-1/2} (\Phi - \Phi_B), \quad (11)$$

$$\frac{dn}{dt} = 0, \quad (12)$$

When Eq. (11) is linearized, the inertial term on the left-hand-side (lhs) contains the drive terms for the centrifugal, Coriolis, and Kelvin-Helmholtz effects. The sheath term on the rhs yields the drive term for the Berk-Ryutov-Tsidulko ∇T_e -driven sheath instability in the eikonal limit.²³ However, we will show that the sheath term turns out to have a net stabilizing effect in the low mode number limit of interest here.

For the linearized stability analysis, we assume a 1D blob equilibrium (varying only in r) and linearize the equations (11) and (12) using the following ansatz:

$$\begin{aligned} n &= \bar{n}(r) + \tilde{n}(r) e^{im\theta} e^{-i\omega t}, \\ \varphi &= \bar{\varphi}(r) + \tilde{\varphi}(r) e^{im\theta} e^{-i\omega t}, \end{aligned} \quad (13)$$

where $\bar{\varphi} = \Phi_B(r)$. Linearizing Eq. (12) gives the following solution for \tilde{n}

$$\tilde{n} = -\frac{m}{r} \frac{\bar{n}'(r)}{\omega - m\Omega} \tilde{\varphi} = -\frac{m}{r} \bar{n}' \psi, \quad (14)$$

where ψ is defined by

$$\tilde{\varphi} = (\omega - m\Omega) \psi. \quad (15)$$

and is related to the radial component of the plasma displacement ξ , viz. $\psi = r\xi_r/m$.

We carry out the linearization of Eq. (11) without the sheath term ($\alpha \rightarrow 0$) and combine the result with Eqs. (14) and (15) to get the usual magnetohydrodynamic (MHD) result

$$\frac{d}{dr} r \bar{n} F \frac{d\psi}{dr} - m^2 \bar{n} F \frac{\psi}{r} - \frac{d}{dr} \left[\bar{n} (F - \omega^2) \right] \psi = 0 , \quad (16)$$

where $F \equiv (\omega - m\Omega)^2$ and $F - \omega^2 = m\Omega(m\Omega - 2\omega)$. After some straightforward algebra, it can be shown that Eq. (16) is equivalent to the form given in Ref. 22

$$\frac{d}{dr} r^3 \bar{n} F \frac{d\xi}{dr} - (m^2 - 1) \bar{n} F r \xi + \frac{d(n\omega^2)}{dr} r^2 \xi = 0 . \quad (17)$$

It is also straightforward to add the sheath conductivity term [α term in Eq. (6)] to the derivation. If one linearizes the sheath term retaining temperature perturbations, $\tilde{T} = -\xi \cdot \nabla \bar{T}$, there is a cancellation of the rotational drift terms, and the stability equation becomes

$$r \frac{d}{dr} r \bar{n} F \frac{d\psi}{dr} - m^2 \bar{n} F \psi - r \frac{d}{dr} \left[\bar{n} (F - \omega^2) \right] \psi - \frac{i\alpha \bar{n} \omega r^2}{\bar{T}^{1/2}} \psi = 0 . \quad (18)$$

In the remainder of the paper, we drop the overbars on all equilibrium quantities. Thus, we have shown that perturbing the "hot blob" model equations yields a generalization of the standard rotational stability equation to include sheath dissipation effects. In the eikonal (high- m) limit, the sheath term is the drive term for the ∇T_e -driven sheath instability.²³

Finally, we examine the dimensionless parameters for the stability problem. Note that the blob radius a can be scaled out of Eq. (18) by the substitutions $r \rightarrow r/a$, $\alpha \rightarrow \alpha a^4$, $\psi \rightarrow \psi/a^2$, $\Omega \rightarrow \Omega a^2$ and $\omega \rightarrow \omega a^2$. Thus, the normalized eigenvalue ωa^2 is independent of a . If we represent the rotation frequency by its value at the radial location where the eigenfunction peaks, $\Omega \rightarrow \Omega_p \sim C_B/a^2$, the blob stability is characterized by two dimensionless parameters, m and $S_\alpha \equiv (\alpha a^4)/(\Omega_p a^2) = (\alpha a^2)/\Omega_p$, describing the mode width and the sheath conductivity, respectively.

IV. Blob Stability Results

A. Linear Stability Analysis

We have applied the formalism of Sec. III to an equilibrium solution for rotating blobs. We choose a Gaussian blob density profile $n(r)$ of unit amplitude

$$n(r) = (1 - \varepsilon) e^{-r^2/(2a^2)} + \varepsilon, \quad (19)$$

where a is the blob radius and ε specifies the relative height of the constant floor density across which the blob propagates. We set $\varepsilon = 0.01$ to ensure a localized solution for the blob potential.¹⁵ The effects of varying the ratio ε on the blob velocity and stability were explored in Ref. 15. The blob's internal electron temperature profile is given by

$$T_e = T_{e0} T(r) = T_{e0} n^v \quad (20)$$

using Eq. (10). We assume that $T = \text{const.}$ along the field lines, implying that the blobs are fully connected to the sheaths and the Bohm sheath potential is given by $\Phi_B(r) = C_B T(r)$, where $C_B \approx 3$. The blob polarization potential due to the curvature drift, $\phi_{\text{pol}}(y) = q \nabla_y \ln n(y)$, which drives its radial motion, is smaller than the Bohm potential ($\phi_{\text{pol}} / \Phi_B \sim r_s / a \ll 1$) and can be neglected in the stability analysis and in computing the rotation. In the $T_i = 0$ limit, the rotation frequency $\Omega(r) \approx \Omega_E(r)$ is proportional to $T(r)$ in the limit $\varepsilon \ll 1$.

In Fig. 1, the profiles $n(r/a)$ and $\Omega(r/a)$ are shown for the base case ($v = 2$). Note that the rotation profile is far from the familiar rigid-rotor limit ($\Omega = \text{const}$) which is often invoked in studying rotational stability. Thus, in addition to purely centrifugal and Coriolis effects, angular-velocity-shear will also play a role in determining the blob stability. This effect can be stabilizing or destabilizing (Kelvin-Helmholtz instability) depending on the parameters.

The eigenfunction $\psi(r)$ is obtained by solving Eq. (18) with $F(r, \omega) = (\omega - m\Omega)^2$, subject to the boundary conditions that $\psi'/\psi = m/r$ as $r \rightarrow 0$ and $\psi'/\psi = -m/r$ as $r \rightarrow \infty$, with $\psi' = d\psi/dr$. The results presented here were obtained using a shooting method to determine the eigenvalue ω by requiring that the logarithmic derivative of ψ be

continuous at an interior matching point. The shooting code has been checked using another code employing a matrix method and by comparison with an analytic solution for a sharp-boundary density, rigid-rotor profile.

First, we consider blob stability in the absence of sheath conductivity ($\alpha = 0$). In Fig. 2 we show a plot of the density profile n/n_0 , the rotational mode instability drive [$\propto (r^2/n) d(n\Omega)/dr$], and the amplitude of the $m = 2$ eigenfunction $|\psi|$ vs r/a for the case $a = 10$ (in units of ρ_s), $\varepsilon = 0.01$, and $\nu = 2$. Each profile is normalized to have a maximum value of approximately unity to illustrate the relative shapes. Note that the $m = 2$ rotational mode eigenfunction $|\psi|(r)$ peaks off axis in the low-density outer region of the blob ($1 < r/a < 2$) where the drive term maximizes. This means that the $m = 2$ rotational mode will not break apart the main body of the blob, but merely throw off its low-density outer mantle, and the effective blob radius a will not be substantially affected. This is illustrated by the 2D simulation discussed in the next section.

Consistent with the $k_{\parallel} = 0$ limit of earlier work,^{19,22} we find that the $m = 1$ rotational mode is marginally stable. The blob rotational modes with $m \geq 3$ are found to be stable. However, the $m = 2$ mode is robustly unstable in the absence of sheath effects. We have also checked the sensitivity of the eigenfrequency to the temperature profile. For the parameters $m = 2$, $a = 10$, $\varepsilon = 0.01$, and $\alpha = 0$, we obtain the following eigenvalues ωa^2 (normalized to be independent of a) as a function of ν : $\omega a^2 = -0.96 + 0.57 i$ for $\nu = 0.5$, $-1.6 + 0.76 i$ for $\nu = 1.0$, and $-2.6 + 0.94 i$ for $\nu = 2.0$. Both the real and imaginary parts of the eigenvalue increase with the temperature gradient parameter ν . We conclude that $\gamma a^2 \sim 1$ and $\gamma a^3 \gg 1$ over a wide range of temperature profiles for $m = 2$.

We have also investigated the effect of the sheath conductivity α on the rotational stability. In Fig. 3, we show γa^2 for $m = 2$ vs the sheath conductivity parameter $S_{\alpha} = \alpha a^2 / \Omega_p$ for the base case temperature profile ($\nu = 2.0$). Here, $\Omega_p \sim C_B / a^2$ is the value of the rotation frequency at the radius r where the eigenfunction peaks, and S_{α} specifies the ratio of the sheath conductivity to the vorticity associated with the rotation. The decrease in growth rate with S_{α} illustrates the stabilizing effect of the sheath conductivity. It was

difficult to find numerical solutions for $S_\alpha \geq 1$ using the shooting algorithm because the eigenfunctions become very localized and the mode eventually stabilizes. In the limit $S_\alpha \ll 1$, the blob spin time around its axis ($\tau_s \sim \Omega^{-1}$) is much shorter than the time for its vorticity (spin or charge) to dissipate by parallel loss ($\tau_\phi \sim 1/\alpha a^2$) and the growth rate is not affected by the presence of the sheaths. Figure 3 shows that stabilization by parallel loss of vorticity to the sheaths requires $S_\alpha = \alpha a^2/\Omega_p > 1$.

In the eikonal or high- m limit ($k_r \sim k_\theta = m/r \gg 1/a$), one can show that Eq. (18) yields the following well-known local dispersion relation^{23,24}

$$(\omega - \omega_E)^2 + i\omega_s \omega = 0, \quad (21)$$

where $\omega_E \equiv m\Omega_E \rightarrow m\Omega$ in the limit $T_i \rightarrow 0$ and $\omega_s = \alpha/k_\perp^2 \rightarrow \alpha r^2/m^2$ for $k_r \ll k_\theta$. This dispersion relation predicts unstable BRT modes driven by the internal temperature-gradient in the limit of high sheath conductivity (S_α). However, more detailed analytic and numerical investigations show that the blob's cylindrical geometry, together with monotonically decreasing $T(r)$ profiles, typically prevents the existence of a "radial well" necessary for localized absolutely-unstable modes in the eikonal limit. Physically, this may be related to the fact that the sheath drive ω_s vanishes at $r = 0$ where the rotation Ω (proportional to the temperature-gradient) maximizes [see Fig. 1].

B. 2D Nonlinear Simulation

In this section, we complement the linear 1D theory presented in Sec. IV by presenting results of a 2D nonlinear simulation of blob transport that solves the following equations

$$\nabla \cdot \left(n \frac{d}{dt} \nabla_\perp \Phi \right) = \alpha n (\Phi - \Phi_B) - \beta \nabla_y n, \quad (22)$$

$$\frac{dn}{dt} + \alpha n = 0, \quad (23)$$

with $\Phi_B = \Phi_{B0}$. All quantities are assumed to be constant along the field lines. The code used was a slight generalization of the one employed in a previous study of blob

instabilities,¹⁶ in that the Bohm sheath term ($\alpha n \Phi_B$) was added on the rhs of the vorticity equation to drive the rotation. This code includes the rotational, curvature and sheath conductivity terms but again neglects FLR effects.

The 2D simulation including the Bohm sheath effects shows good agreement with the 1D stability results described in the previous section. This is illustrated by a snapshot shown in Fig. 5 of a case with parameters $a = 10$, $\alpha = 3 \times 10^{-5}$, $\beta = 6.9 \times 10^{-4}$ and $\Phi_{B0} = 10$, so that $S_\alpha \approx \alpha a^4 / \Phi_{B0} = 0.03$. The blob develops an $m = 2$, $k_{\parallel} = 0$ instability on a timescale short compared to the theoretical convection time $\tau_c = a/v_x$, i.e. $\gamma a^3 \gg 1$, in agreement with the linear stability analysis. The frame in Fig. 5 occurs after about one τ_c and shows that the instability has undergone several e-foldings to produce an observable distortion of the blob. The instability peaks near the outside of the blob, as predicted by the linear stability analysis, and throws off an outer shell of material that wraps around to form a "halo" or "tail". The tail is left behind by the blob's rotation and curvature-driven propagation to the right. The instability shown here is clearly rotational in origin and differs qualitatively from the curvature-driven blob instabilities studied earlier.^{15,16} The appearance of the rotational instability in this run is consistent with the conditions $S_\alpha \ll 1$ and $m < (C_B a/q)^{1/2}$ discussed in previous sections. A similar run with $a = 30$, implying $S_\alpha = 2.4$, was also unstable, but the instability had a different character (not shown here). This is in agreement with the present theory, where $S_\alpha \geq 1$ implies strong stabilization of the rotational branch.

We remark in passing that the blob dynamics (e.g. temporal variation of v_x and v_y) at later times is very interesting in the simulation corresponding to Fig. 5, as other rotational effects¹⁴ come into play. For example, the radial velocity of the blob is observed to increase after throwing off its outer mantle and it develops a poloidal velocity. A complete description of the simulation results will be presented elsewhere.²⁵

V. Summary and Discussion

In this paper, we have studied the rotational stability of blobs with interiors hotter than the surrounding plasma. The study of temperature profile effects in blobs is partly

motivated by recent observations that ELMs produce blob-like transport.^{9,17,18} Large ELMs are typically associated with high-confinement H-modes, which have hot pedestals and SOL plasmas which are attached to the divertor plates. Under these conditions, the blobs produced by the ELM crashes are expected to have substantial size, to be connected to the divertor sheaths, and to transport energy as well as particles. Another motivation of this study is to obtain a visual "signature" for blob spin (or equivalently, sheath connection) that would be helpful in the analysis of the 2D data from gas puff imaging (GPI) diagnostics on various tokamaks.^{10,12}

The main results of this paper are:

- 1) For typical internal density and electron temperature profiles with $T_i = 0$, blobs are linearly unstable only to the $m = 2, k_{\parallel} = 0$ mode in the absence of sheath conductivity; the growth time of this mode (γ^{-1}) is typically much faster than the blob transport time $\tau_c = a/u_x \sim a^3$, i.e. $\gamma \tau_c \sim \gamma a^3 \gg 1$.
- 2) The $m = 2$ eigenfunction peaks in the low-density outer part of the blob and does not affect the blob size very much, other than to throw off a tenuous outer mantle [see Fig. 4].
- 3) When $T_i \neq 0$, the $\mathbf{E} \times \mathbf{B}$ and diamagnetic drifts reinforce each other for typical blob profiles, so that FLR stabilization does not occur for the parameters expected in the tokamak SOL.
- 4) Sheath conductivity stabilizes the rotational mode when $S_{\alpha} \equiv \alpha a^2 / \Omega_p > 1$, where α is the sheath conductivity parameter, a is the blob radius, and $\Omega_p \sim C_B / a^2$ is the rotation frequency at the radial location where the eigenfunction peaks.
- 5) For finite sheath conductivity, the stability equation includes the Berk-Ryutov-Tsidulko ∇T_e instabilities in the eikonal limit (driven by the internal blob temperature profile), but these modes are stable for the low mode numbers of interest here.

Based on this analysis, we conclude that blob rotational instabilities differ from curvature-driven ones¹⁴⁻¹⁶ in several respects. The low- m curvature-driven modes cause blob bifurcation, reducing the blob size a and increasing its radial velocity, $v_x = q/a^2$. (The charge polarization occurs over a distance of order a so that the polarization

potential scales as $\phi \sim 1/a$ and the resulting electric field as $E_y \sim 1/a^2$.) In contrast to this situation, the unstable $m = 2$ rotational mode peaks farther out in radius [Fig. 2] and does not affect the high-density part of the blob. This leads us to conclude that the effect of rotational *instability* on the particle and energy transport is small, although rotational *charge mixing*¹⁴ in the blob can greatly reduce the transport. The $m = 2$ rotational instability causes the blob to shed particles from its outer low-density mantle and to deform in shape [Fig. 4]. The pinwheel shape shown in Fig. 4 is characteristic of this mode, differing both from the bifurcation events¹⁵ induced by curvature-driven modes and from the mushroom shapes¹⁶ observed in simulations of the Kelvin-Helmholtz instability, and may serve as a useful signature of blob spin (and sheath connection) in the analysis of the 2D GPI data.

It is useful to examine the characteristic length scales of the various instabilities. Previously numerical simulations showed that the Kelvin-Helmholtz instability driven by $v_x(y)$ is dominant for $a \ll a_*$, whereas the curvature-driven sheath-interchange mode is observed when $a \gg a_*$.¹⁶ Here, $a_* = (q/\alpha)^{1/5}$ is the fundamental blob scale in the absence of spin and dissipation, for which the inertial, sheath and curvature terms balance in the vorticity equation. Assuming $a = a_*$ to obtain a maximal ordering, we can write the condition that the $m = 2$ rotational mode growth rate be larger than the curvature-driven mode [Eq. (5)] in the form $a_* < a_{sh} = (C_B/\alpha)^{1/4}$. Here, the quantity a_{sh} is the scale length at which sheath conductivity stabilization of rotational modes becomes effective, i.e. $S_\alpha = 1$ implies $a = a_{sh}$. For a wide range of tokamak parameters, one finds that $a_* \leq a_{sh}$. Thus, in practice curvature, rotational, and sheath effects all play a role in determining the blob stability.

To put this work in a broader context, we note that there has been recent progress in the understanding of 2D blob transport under the action of curvature^{2,3} and rotation,¹⁴ and the extension of the blob transport model to the 3D collisional regime.²⁶ This work needs to be supplemented by studies of blob creation and destruction (e.g. by secondary instabilities) to determine the effective transport. With the present paper, we now have an understanding of secondary instabilities due to curvature, velocity shear, and rotation,

which should provide a good foundation for comparing the blob model with large scale turbulence simulations and experimental data.

Acknowledgements

This work was supported by the U.S. Department of Energy (DOE) under DOE Grants No. DE-FG03-97ER54392 and DE-FG03-00ER54568; however, this support does not constitute an endorsement by the DOE of the views expressed herein.

References

- ¹ W. Horton, Phys. Fluids B **1**, 524 (1989).
- ² S. I. Krasheninnikov, Phys. Lett. A **283**, 368 (2001).
- ³ D. A. D'Ippolito, J. R. Myra, and S. I. Krasheninnikov, Phys. Plasmas **9**, 222 (2002).
- ⁴ S. J. Zweben, Phys. Fluids **28**, 974 (1985).
- ⁵ M. Endler, H. Niedermeyer, L. Giannone, E. Holzhauser, A. Rudyj, G. Theimer, N. Tsois and ASDEX team, Nucl. Fusion **35**, 1307 (1995).
- ⁶ R. A. Moyer, R. D. Lehmer, T. E. Evans, R. W. Conn, and L. Schmitz, Plasma Phys. Contr. Fusion **38**, 1273 (1996).
- ⁷ M. Umansky, S. I. Krasheninnikov, B. LaBombard and J. L. Terry, Phys. Plasmas **5**, 3373 (1998); B. LaBombard, M. V. Umansky, R. L. Boivin, J. A. Goetz, J. Hughes, B. Lipschultz, D. Mossessian, C. S. Pitcher, J. L. Terry, Alcator Group, Nucl. Fusion **40**, 2041 (2000).
- ⁸ G. Y. Antar, P. Devynck, X. Garbet, and S. C. Luckhardt, Phys. Plasmas **8**, 1612 (2001); G. Y. Antar, S. I. Krasheninnikov, P. Devynck, R. P. Doerner, E. M. Hollmann, J. A. Boedo, S. C. Luckhardt and R. W. Conn, Phys. Rev. Letters **87**, 065001 (2001).
- ⁹ J. Boedo, D. Rudakov, R. Moyer, *et al.*, Phys. Plasmas **8**, 4826 (2001); D. L. Rudakov, J. A. Boedo, R. A. Moyer, *et al.*, Plasma Phys. Contr. Fusion **44**, 717 (2002).
- ¹⁰ S. Zweben, D. P. Stotler, J. L. Terry, *et al.*, Phys. Plasmas **9**, 1981 (2002); S. Zweben, R. Maqueda, D.P. Stotler, *et al.*, Nucl. Fusion **44**, 134 (2004).
- ¹¹ J. Neuhauser, D. Coster, H. U. Fahrback, *et al.*, Plasma Phys. Contr. Fusion **44**, 855 (2002).
- ¹² J. L. Terry, S. J. Zweben, K. Hallatschek, *et al.*, Phys. Plasmas **10**, 1739 (2003).
- ¹³ D. A. D'Ippolito, J. R. Myra, S. I. Krasheninnikov, G. Q. Yu, and A. Yu. Pigarov, Contrib. Plasma Phys **44**, 205 (2004).
- ¹⁴ "Convective Transport in the Scrape-Off-Layer by Non-Thermalized Spinning Blobs", J. R. Myra, D. A. D'Ippolito, S. I. Krasheninnikov, and G. Q. Yu, to be published in Phys. Plasmas (2004).

- ¹⁵ D. A. D'Ippolito and J. R. Myra, *Phys. Plasmas* **10**, 4029 (2003).
- ¹⁶ G. Q. Yu and S. I. Krasheninnikov, *Phys. Plasmas* **10**, 4413 (2003).
- ¹⁷ M. Endler, S. Davies, I. Garcia-Cortes et al., in *Proceedings of the 29th EPS Conference on Plasma Phys. and Control. Fusion*, Montreux, Switzerland, 2002, edited by R.Behn and C. Varandas (European Physical Society, Paris, 2002), *Europhysics Conference Abstracts Vol. 26B*, paper O-3.24.
- ¹⁸ B. Gonçalves, C. Hidalgo, M. A. Pedrosa et al., *Plasma Phys. Control. Fusion* **45**, 1627 (2003).
- ¹⁹ J. B. Taylor, *J. Nucl. Energy Pt. C*, **4**, 406 (1962);
- ²⁰ M. N. Rosenbluth and A. Simon, *Phys. Fluids* **8**, 1300 (1965).
- ²¹ L. D. Pearlstein and N. A. Krall, *Phys. Fluids* **9**, 2231 (1966).
- ²² J. P. Freidberg and L. D. Pearlstein, *Phys. Fluids* **21**, 1207 (1978).
- ²³ H. L. Berk, D. D. Ryutov, and Yu. A. Tsidulko, *Phys. Fluids B* **3**, 1346 (1991).
- ²⁴ J. R. Myra, D. A. D'Ippolito, and J. P. Goedbloed, *Phys. Plasmas* **4**, 1330 (1997).
- ²⁵ G. Q. Yu and S. I. Krasheninnikov, private communication (2004).
- ²⁶ "Blob Dynamics in 3D BOUT Simulations of Tokamak Edge Turbulence," D. A. Russell, D. A. D'Ippolito, J. R. Myra, W. M. Nevins, and X. Q. Xu, LRC report LRC-04-99, submitted to *Phys. Rev. Letters* (2004).

Figure Captions

- Fig. 1 Plots of the blob density profile $n(r)$ (solid line) and the rotation frequency profile $|\Omega(r)|$ in arbitrary units (short dashed line), with all profiles normalized to have a maximum value of unity. The parameters are $a = 10$, $\varepsilon = 0.01$, $\nu = 2$, and $\alpha = 0$.
- Fig. 2 Plots of the blob density profile $n(r)$ (solid line), rotational drive $(r^2/n) d(n\Omega)/dr$ (long dashed line), and eigenfunction $|\psi(r)|$ (short dashed line), with all profiles normalized to have a maximum value of order unity. The parameters are $m = 2$, $a = 10$, $\varepsilon = 0.01$, $\nu = 2$, and $\alpha = 0$.
- Fig. 3 Plot of the $m = 2$ normalized growth rate γa^2 vs the sheath parameter $\alpha a^2/\Omega_p$ for the base case temperature profile ($\nu = 2.0$) with $\varepsilon = 0.01$. The decrease in growth rate with $\alpha a^2/\Omega_p$ illustrates the stabilizing effect of the sheath conductivity α . Blob rotational effects are important when $\alpha a^2/\Omega_p \ll 1$, where Ω_p is the value of the rotation frequency at the radius where the eigenfunction peaks.
- Fig. 4 Snapshot of a spinning blob taken from a 2D simulation solving Eqs. (22) and (23) for the parameters $a = 10$, $\alpha = 3 \times 10^{-5}$, $\beta = 6.9 \times 10^{-4}$ and $\Phi_{B0} = 10$. This frame shows the development of an $m = 2$ instability with $\gamma \sim \Omega$. The instability peaks near the edge of the blob and throws out a thin mantle of plasma. At later times in the simulation, this mantle is left behind as the blob spins and translates to the right.

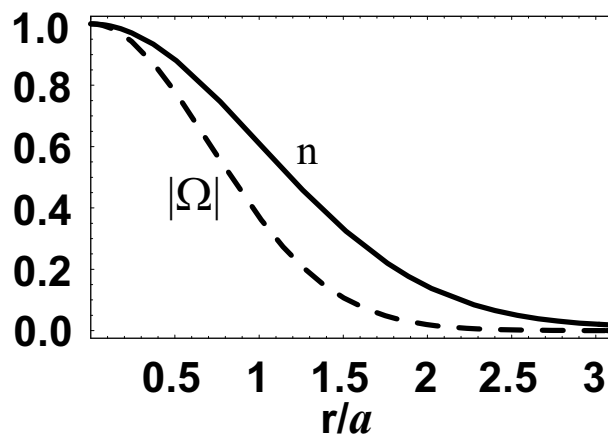


Fig. 1 Plots of the blob density profile $n(r)$ (solid line) and the rotation frequency profile $|\Omega(r)|$ in arbitrary units (short dashed line), with all profiles normalized to have a maximum value of unity. The parameters are $a = 10$, $\varepsilon = 0.01$, $\nu = 2$, and $\alpha = 0$.

Fig 1

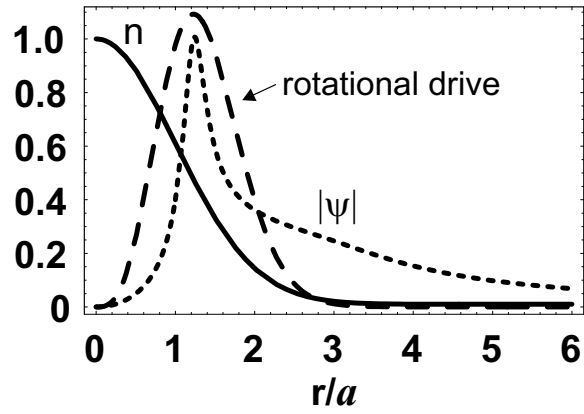


Fig. 2 Plots of the blob density profile $n(r)$ (solid line), rotational drive $(r^2/n) d(n\Omega)/dr$ (long dashed line), and eigenfunction $|\psi(r)|$ (short dashed line), with all profiles normalized to have a maximum value of order unity. The parameters are $m = 2$, $a = 10$, $\varepsilon = 0.01$, $\nu = 2$, and $\alpha = 0$.

Fig 2

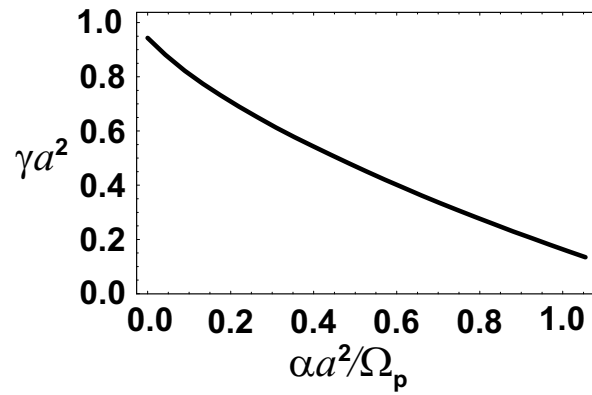


Fig. 3 Plot of the $m = 2$ normalized growth rate γa^2 vs the sheath parameter $\alpha a^2 / \Omega_p$ for the base case temperature profile ($\nu = 2.0$) with $\varepsilon = 0.01$. The decrease in growth rate with $\alpha a^2 / \Omega_p$ illustrates the stabilizing effect of the sheath conductivity α . Blob rotational effects are important when $\alpha a^2 / \Omega_p \ll 1$, where Ω_p is the value of the rotation frequency at the radius where the eigenfunction peaks.

Fig 3

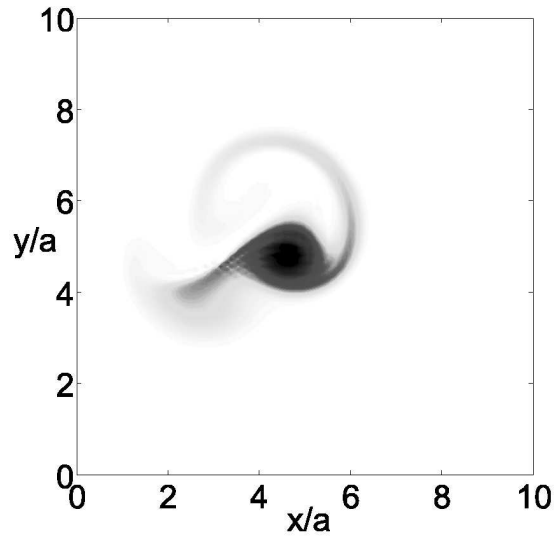


Fig. 4 Snapshot of a spinning blob taken from a 2D simulation solving Eqs. (22) and (23) for the parameters $a = 10$, $\alpha = 3 \times 10^{-5}$, $\beta = 6.9 \times 10^{-4}$ and $\Phi_{B0} = 10$. This frame shows the development of an $m = 2$ instability with $\gamma \sim \Omega$. The instability peaks near the edge of the blob and throws out a thin mantle of plasma. At later times in the simulation, this mantle is left behind as the blob spins and translates to the right.

Fig 4